AD_____

Award Number:
W81XWH-09-1-0410

TITLE:
Harnessing the power of light to see and treat breast cancer

PRINCIPAL INVESTIGATOR:
Nirmala Ramanujam, Ph.D.

CONTRACTING ORGANIZATION:
Duke University

Durham, NC 27708

REPORT DATE:
October, 2010

TYPE OF REPORT:
Annual

PREPARED FOR: U.S. Army Medical Research and Materiel Command
Fort Detrick, Maryland 21702-5012

DISTRIBUTION STATEMENT:

X Approved for public release; distribution unlimited

REPORT DOCUMENTATION PAGE

Form Approved
OMB No. 0704-0188

1. REPORT DATE *(DD-MM-YYYY)*	**2. REPORT TYPE**	**3. DATES COVERED** *(From - To)*
01-10-2010	Annual	18 Sep 2009 - 17 Sep 2010

4. TITLE AND SUBTITLE

Harnessing the power of light to see and treat breast cancer.

5a. CONTRACT NUMBER

5b. GRANT NUMBER
W81XWH-09-1-0410

5c. PROGRAM ELEMENT NUMBER

6. AUTHOR(S)

Nirmala Ramanujam, Ph.D.

5d. PROJECT NUMBER

5e. TASK NUMBER

5f. WORK UNIT NUMBER

7. PERFORMING ORGANIZATION NAME(S) AND ADDRESS(ES)

Duke University

Durham, NC 27708

8. PERFORMING ORGANIZATION REPORT NUMBER

9. SPONSORING / MONITORING AGENCY NAME(S) AND ADDRESS(ES)
U.S. Army Medical Research
And Material Command

Fort Detrick, Maryland 21702-
5012

10. SPONSOR/MONITOR'S ACRONYM(S)

11. SPONSOR/MONITOR'S REPORT NUMBER(S)

12. DISTRIBUTION / AVAILABILITY STATEMENT

Approved for public release; distribution unlimited.

13. SUPPLEMENTARY NOTES

14. ABSTRACT

Our objective is to exploit the wealth of physiological, metabolic, morphological and molecular sources of optical contrast to develop novel strategies that focus on two breast cancer applications: tumor margin assessment and prediction of response to neo-adjuvant therapy. The proposed aims of this grant are expected to result in three major contributions. The first has the most immediate impact. An optically based strategy that can quickly and non-destructively detect positive tumor margins will decrease the need for re-excision surgery and thereby decrease the local recurrence rate and rate of distant metastases in women electing BCS. Gaining insight into the physiological, metabolic, morphological and molecular sources of heterogeneity within and among tumors and how they are modulated by therapy, drug resistance and metastatic potential will directly benefit prognostication, prediction of outcome and planning of cancer therapies. With these tools, clinicians and clinical researchers can get a better understanding of this disease and how it might react to a drug. Basic science researchers could use it as an informed approach to study tumor biology and assay the effect of novel therapeutic agents *in vivo*.

15. SUBJECT TERMS
optical spectroscopy, imaging, fiber-optic, molecular, screening, breast cancer

16. SECURITY CLASSIFICATION OF:			**17. LIMITATION OF ABSTRACT**	**18. NUMBER OF PAGES**	**19a. NAME OF RESPONSIBLE PERSON**
a. REPORT	**b. ABSTRACT**	**c. THIS PAGE**			USAMRMC
U	U	U	UU	30	**19b. TELEPHONE NUMBER** *(include area code)*

Table of Contents

1. INTRODUCTION:

Our objective is to exploit the wealth of physiological, metabolic, morphological and molecular sources of optical contrast to develop novel strategies that focus on two breast cancer applications: tumor margin assessment and prediction of response to neo-adjuvant therapy. The proposed aims of this grant are expected to result in three major contributions. The first has the most immediate impact. An optically based strategy that can quickly and non-destructively detect positive tumor margins will decrease the need for re-excision surgery and thereby decrease the local recurrence rate and rate of distant metastases in women electing BCS. Gaining insight into the physiological, metabolic, morphological and molecular sources of heterogeneity within and among tumors and how they are modulated by therapy, drug resistance and metastatic potential will directly benefit prognostication, prediction of outcome and planning of cancer therapies. With these tools, clinicians and clinical researchers can get a better understanding of this disease and how it might react to a drug. Basic science researchers could use it as an informed approach to study tumor biology and assay the effect of novel therapeutic agents *in vivo*.

a. Original Statement of Work for 5 Years

Aim 1: Optical imaging of margin morphology on breast lumpectomy specimens: To evaluate the role of wide-field imaging (coverage) and high-resolution interrogation (localization) of breast margin morphology to guide surgical resection intra-operatively and pathologic assessment of the tumor margin post-operatively (Timeframe: year 1-5).

1a. Development of one optical spectral imaging system that integrates sensing capabilities for aims 1 and 2 and a high-resolution probe that can image absorption, scattering and fluorescence contrast (timeframe, year 1).

1b. Conduct clinical studies on lumpectomy margins on 200 patients (time frame, years 2-4)

1c. Data analysis and interpretation (timeframe, years 3-5)

Test the sensitivity and specificity of wide-field imaging to detect positive tumor margins

Test sensitivity and specificity of high-resolution probe to detect IDC and DCIS.

Aim 2: Optical quantitative biology of different sub-types of breast cancer: To investigate biomarkers of oxygenation, carotenoids (β-carotene) and ECM proteins (collagen) in human breast cancer stratified by tumor sub-type and receptor status and their association with neo-adjuvant chemotherapy response.

2a. Development of rotating needle compatible spectroscopy probe (timeframe, year 1).

2b.Conduct clinical studies to measure optical biomarkers *in vivo* in 150 patients undergoing surgery (timeframe, years 2-4).

2c. Conduct clinical studies to measure optical biomarkers from 75 patients before neo-adjuvant therapy

2d. Data analysis and interpretation (years 3-5):

Determine association of biomarkers with tumor subtype

Determine association of biomarkers with receptor status

Determine association of biomarkers with genomic signatures

Determine association of biomarkers with pathologic sub-total and complete response

Aim 3: Optical quantitative biology to assess therapy response in different sub-types of breast cancer: To investigate biomarkers of oxygenation and ECM proteins (collagen and $\alpha_v\beta_3$ expression) in rodent breast cancer stratified by tumor sub-type, receptor status and metastatic potential in response to targeted and chemotherapies.

3a. To determine if multi-parametric intra-vital optical microscopy, measuring hemoglobin saturation, total hemoglobin, redox ratio, collagen, and integrin expression can monitor tumor response to tamoxifen in parental and tamoxifen-resistant MCF-7 tumors in the mouse dorsal skin fold window chamber (timeframe, years 1-2).

- A total of 40 athymic nude mice will be required for this study (10 mice/group).

3b. Monitor optical parameters in the dorsal skin fold window chamber in response to doxorubicin chemotherapy in MCF-7 parental and doxorubicin-resistant tumors (timeframe, years 2-3).

- A total of 40 athymic nude mice will be required for this study.

3c. Monitor optical parameters in the dorsal skin fold window chamber in response to doxorubicin chemotherapy in tumors that express high (MDA-435) and low (MCF-7) levels of $\alpha_v\beta_3$ integrin (timeframe, years 3-4).

- A total of 40 athymic nude mice will be required for this study.

3d. Data and statistical analysis (timeframe, year 5).

2. BODY:

Aim 1: Optical imaging of margin morphology on breast lumpectomy specimens

A. High resolution imaging component: High resolution imaging of tumor resection margins

In Aim 1, our objective is to develop a strategy for high resolution fluorescence imaging of tumor margins, and to combine that with wide-field diffuse spectral imaging in a complementary fashion. For the high resolution fluorescence imaging component of the project, our first step was to evaluate the feasibility of high resolution fluorescence imaging for detection of residual carcinoma in the normal tissue milieu. We are demonstrating this in 2 *ex vivo* testbeds: 1) murine sarcoma margins and 2) human mastectomy specimens. Each of these approaches is subsequently discussed in more detail.

Introduction: One strategy for accurate assessment of tumor margins is to exploit features that are already leveraged in traditional pathology, such as nuclear size and density, or relationships between tumor cells and surrounding support structures (collagen, fat, muscle) [1]. Recent advances in optical imaging coupled with contrast agents enable such visualization of microscopic features without extensive pathologic processing. In particular, Richards-Kortum et al. have developed a high resolution fluorescence microendoscope (HRME) and used it in

conjunction with acriflavine, a vital fluorescent nuclear stain, to image dysplasia and early cancer in the oral cavity and esophagus [2,3]. While this tool has been used to diagnose cancer in these sites, its potential to determine margin status has not been explored. Therefore, we completed a pilot feasibility study is to evaluate the potential of HRME and acriflavine in the context of surgical margins, specifically to see if this tool can detect the presence of microscopic disease at margins intraoperatively without the need for time-intensive tissue processing.

Our ultimate objective is to use the wide-field spectral imaging device to identify suspicious areas on breast lumpectomy specimens, which will then be evaluated in high resolution with the high-resolution microendoscope (HRME). However, we acknowledge that detecting the small focal areas of residual cancer that characterize lumpectomy margins poses challenges and is therefore not the optimal setting in which to complete preliminary validation studies of high resolution imaging for surgical margins. Therefore, we chose to begin with a pilot study of murine sarcoma margins in addition to a small pilot study on mastectomy specimens. The murine pilot study allows us to obtain a number of images of the natural border between the solid tumor and the surrounding normal tissue and allows us to confirm that HRME imaging can detect residual carcinoma against a background of normal tissue with an adequate number of samples to evaluate this capability. The small pilot study on mastectomy margins allows us to more quickly assemble a "library" of representative high resolution fluorescence images (including invasive and *in situ* cancers), than we would not be able to readily obtain had we started with breast lumpectomy margins due to the small subset of malignant images that would be acquired. Having representative images from all types of tissue present in the breast will be important for evaluating the potential of this type of imaging for detecting residual breast cancer, and will help us to determine whether any additional modifications or improvements must be made to the device prior to commencement of the 200 patient lumpectomy study.

1) *Ex vivo* murine sarcoma margins study

Though our lab is most familiar with breast cancer margins, we chose to initially validate the ability of HRME to detect residual disease in the context of a well-characterized transgenic murine sarcoma model [4] because (1) transgenic tumors, which exhibit the problematic in-growths of tumor tissue into surrounding tissue, are better suited for margin imaging than implanted or chemically induced tumors, which grow within a fibrous capsule, and (2) we have access to a well-characterized sarcoma model at Duke from our collaborator in radiation oncology, Dr. David Kirsch.

Methods:

Instrumentation: The HRME device has previously been described in detail [3]. The system contains a 455 nm light emitting diode (LED) to excite acriflavine. Light is directed by a dichroic mirror through the 10x/ 0.25 NA infinity corrected objective lens to the coherent fiber bundle. The fiber bundle is composed of 30,000 fibers giving a circular field of view of approximately 750 um in diameter. Light reflected from the sample is collected by the fiber bundle and directed back through a 475 nm cut-off dichroic mirror and imaged onto a CCD camera by a tube lens. Images are produced by placing the fiber bundle in contact with the tissue surface and can be viewed on a computer in real-time. Based on the spacing and size of individual fibers in the fiber bundle, the system has a resolution of approximately 4 um.

Imaging protocol: All murine work was performed in accordance with Duke University Institutional Animal Care and Use Committee approved protocols. Within ten minutes of

euthanasia, tumors were removed and sliced into three sections: proximal, middle, or distal to the body of the mouse. An additional slice was taken from the tumor bed and from the contralateral leg (benign tissue). Sections were laid flat followed by topical application of 0.01% (w/v) acriflavine (Sigma-Aldrich) dissolved in phosphate buffered saline (PBS). Acriflavine is a fluorescent molecule that reversibly binds with nucleic acids thereby facilitating visualization of cell nuclei and other tissue components [5].The distal end of the HRME fiber bundle was placed in contact with the tissue and images were acquired. In a few cases tissue slices were raster-scanned to create mosaics of the tissue face by systematically moving the probe in 1 mm increments in rows over the tissue surface. In order to improve the accuracy and reproducibility of these movements the probe was secured in a custom fiber chuck which was mounted on an x-y translation stage. Between each probe placement the distal end of the probe was cleaned with 55% ethanol.

Pathological coregistration: During the imaging session specific sites of interest were inked with 1 mm dots for pathologic coregistration. For the mosaics, the four corners of the scanned area were inked and an *en face* section was taken during histopathological processing such that the tissue in between the dots could be visualized (Figure 3). After imaging and inking was complete, the tissue was returned for standard pathologic processing, and the resulting hematoxylin and eosin (H&E) stained slides were reviewed by an expert oncology pathologist and an expert veterinary pathologist, both of whom were blinded to the results of HRME imaging. For each inked area a diagnosis was given, which included tumor, muscle, and adipose tissue or any combination thereof.

Image analysis: HRME images were reviewed to determine whether the probe was in adequate contact with the tissue surface across the image or whether artifacts were present, such as motion artifact or hair artifacts. Images with these artifacts were removed from the image set and not used in further analysis.

A training set comprising 5 malignant and 7 benign example images with corresponding pathology were shown to two certified pathologists and two additional reviewers (Table 1). Immediately afterwards, reviewers were shown a separate set of 24 malignant and 21 benign test images and asked to score them according to tissue type (muscle, adipose, tumor, or a combination). Any diagnosis with ‘tumor’ present was considered positive while those with just ‘muscle’ and/or ‘adipose’ were considered negative. Images with mixed morphologies were similarly considered—those with ‘tumor + muscle’ or ‘tumor + adipose’ were considered positive and those with ‘muscle + adipose’ were considered negative. Results were compared to the gold-standard pathologic diagnosis at each site, and diagnostic accuracy was calculated for each reviewer.

In addition to qualitative image analysis, a preliminary quantitative image analysis was performed. Homogeneous regions of interest (ROI) that are representative of a given tissue type were selected and image parameters such as standard deviation, entropy, kurtosis, and skewness were calculated from raw pixel values within that region. While several of these raw features have previously been shown to have good diagnostic performance at distinguishing neoplastic from nonneoplastic tissue in the esophagus [2], we wanted to extend our analysis further to look at parameters that captured morphological characteristics of tissue types. To do so we converted the gray scale images to binary masks utilizing Otsu's method, which chooses a threshold to minimize the intraclass variance of the black and white pixels. From the binary images, parameters such as size or density of features or the distance between features (nearest neighbor calculated through the Euclidean distance transform) were calculated.

In addition to calculating these features from the original image, we are exploring the effect of image pre-processing steps on creation of the binary masks and the resulting quantitative image parameters. In particular we are interested in characterizing the frequency content of homogeneous images in order to understand which frequency components are associated with muscle, tumor, and adipose and consequently use this information to isolate which tissue types are present through filtering methods. An example of the utility of such an approach is shown in figure 5.

Results:

Representative images: Seven animals were used in the pilot study yielding a total of 55 images with a concordant pathological diagnosis. Figure 1 shows representative HRME images of homogeneous tissues (single tissue type within the image area), along with their corresponding *en face* H&E section micrographs. For comparison all images are at the same magnification. Densely packed, disorganized nuclei, typical of sarcomas, can be readily seen in Fig. 1A and Fig. 1B. Contrastingly, the muscle seen in Fig. 1C and Fig. 1D is mostly devoid of the small round nuclei. Rather, one can see distinct muscle fibers both in cross section (Fig. 1C) and in a longitudinal section (Fig. 1D). Large round adipocytes characteristic of adipose tissue are clearly seen in Fig. 1E.

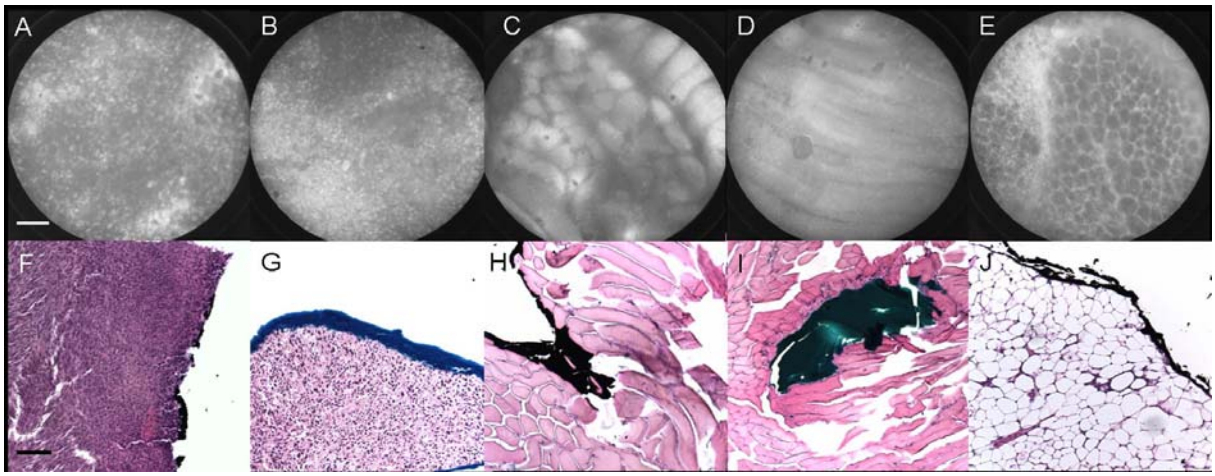

Figure 1. Representative images of A-B) tumor, C) muscle in cross section, D) muscle in longitudinal section, E) adipose tissue and F-J) corresponding *en face* histological images. Scale bar 100 µm.

Figure 2 illustrates HRME images of heterogeneous tissues (mixed muscle and tumor morphologies) along with their corresponding *en face* H&E section micrographs. For comparison all images are at the same magnification. In the H&E images tumor is infiltrating the muscle, which is a typical feature of positive surgical sarcoma margins. This is reflected in the HRME images in which distinct tumor and muscle areas are seen.

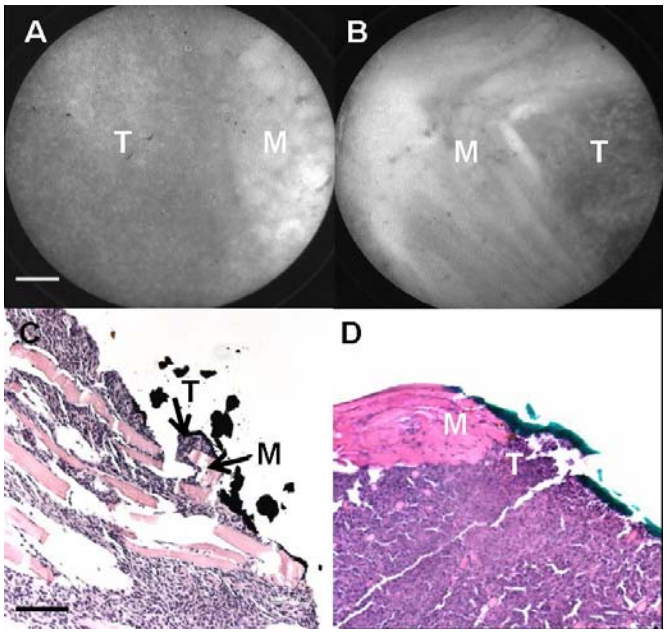

Figure 2. Images with mixed muscle and tumor morphologies and C-D) corresponding *en face* histological images. T indicates tumor and M indicates muscle. Scale bar 100 μm.

To illustrate that the HRME can give an accurate picture of margin status on a larger scale, we stepped the probe across an excised sarcoma specimen in 1 mm increments through use of a translation stage. Figure 3 contains a panel of representative high-resolution fluorescence images, a photograph of the tumor with inks for orientation, and the corresponding H&E *en face* section micrograph. For pathologic co-registration, the four corners of the imaged area were inked, and the diagnosis of these areas was read on the resulting H&E histology slide (shown in Fig. 3C). The lower right image in Fig. 3A clearly contains muscle fibers, which was confirmed in the H&E slide, as was the presence of tumor in the upper right image. The lower left image in Fig. 3A shows both tumor nuclei and muscle fibers, which was also confirmed by pathology.

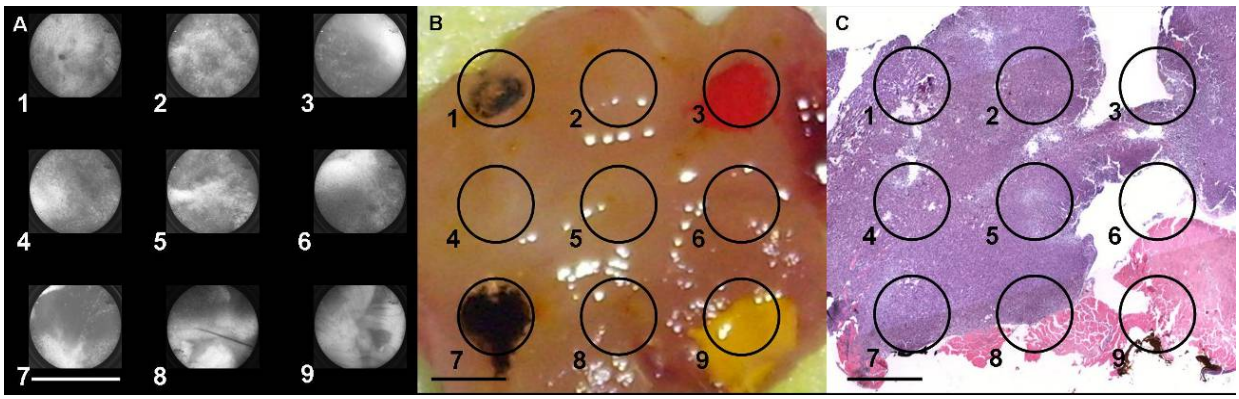

Figure 3. A) Images of excised sarcoma taken by translating the HRME over the tissue. B) The 4 corners of the tissue (corresponding to images 1, 3, 7, 9) were inked for pathologic correlation. C) An *en face* H&E section of the tissue in B is shown. The specific locations where HRME images were collected are indicated by circles in B and C. The tissue types in the path slide correspond with the tissue types observed in the HRME images. For instance, the lower right

yellow dot was on muscle tissue, whereas muscle fibers are clearly seen in the corresponding HRME image. Scale bar 1 mm.

Qualitative image analysis: Two expert pathologists and two additional reviewers were trained on a set of 12 representative tumor, muscle, and adipose images marked with the pathologic diagnosis, and were subsequently asked to provide a diagnosis for a test set of 43 HRME images (Table 1). Each reviewer's subjective diagnosis was compared to the corresponding H&E gold standard for that site. The two expert pathologists achieved an average sensitivity and specificity of 93% and 73% respectively. The two additional reviewers achieved an average sensitivity of 93% and specificity of 68% yielding a total average of 93% sensitivity and 71% specificity for all four reviewers (Table 2). Table 3 illustrates the most commonly correctly diagnosed and most commonly misdiagnosed tissue types as assessed by Pathologist 1. For this analysis, any diagnosis with 'tumor' present was considered malignant while those with just 'muscle' and/or 'adipose' were considered benign diagnoses. Images were listed under agreement if both the subjective analysis from HRME images and the pathological diagnosis were evaluated as malignant or if both were considered benign. For example, if the pathologic diagnosis is 'tumor and muscle' and the HRME diagnosis is 'tumor' it is considered an agreement since the goal is to detect the presence of disease. Of the 2 'Tumor + Muscle' disagreements, 1 was incorrectly identified as 'Muscle + Adipose' and 1 as 'Muscle'. Out of the 6 'Muscle' disagreements 4 were incorrectly identified as 'Tumor' and 2 as 'Tumor + Adipose'. As shown, images with mixed morphologies had the lowest percent concordance.

Table 1. Pathologic diagnosis of images in the training and test sets

Tissue type	Training set	Test set	Total
Malignant	5	21	26
Tumor	4	16	20
Tumor + Muscle	1	5	6
Benign	7	22	29
Muscle	6	20	26
Adipose	1	1	2
Muscle + Adipose	0	1	1
Total	12	43	55

Table 2. Qualitative image analysis

	Pathologist1	Pathologist2	Reviewer1	Reviewer2
Sensitivity	90%	95%	95%	90%
Specificity	73%	73%	77%	59%
n	43	43	43	43

Table 3. Qualitative diagnosis vs. pathology gold standard (Pathologist 1)

Tissue type	Agreement	Disagreement	Concordance
Malignant	19	2	90%
Tumor	16	0	100%
Tumor + Muscle	3	2	60%
Benign	16	6	73%
Muscle	14	6	70%
Adipose	1	0	100%
Muscle + Adipose	1	0	100%
Total	35	8	81%

Preliminary quantitative image analysis: Moving forward, our goal is to develop automated feature extraction algorithms to identify HRME image features that discriminate positive from negative margins. In particular we are interested in optimizing pre-processing methods and subsequent analysis that can isolate tumor cells from normal milieu, which is the situation typically encountered at surgical margins. As seen in the qualitative analysis, only 60% of images with both tumor and muscle present were diagnosed correctly (table 3), which further emphasizes the need for a quantitative image analysis approach that can correctly diagnose images that contain residual tumor cells. Thus far, our approach for image classification has focused parameters that capture the raw features of an image, such as mean intensity, standard deviation, skewness, and entropy, and on parameters that capture morphological features, such the size and density of features and spacing of features. One approach that we have explored for calculating morphological features is to convert the grayscale images to binary images through using different thresholding techniques. Figure 1 illustrates how regions of interest, outlined in red, were selected within homogeneous images and then converted to binary images. Once images were in a binary format, parameters that capture morphological characteristics of each tissue type could be calculated.

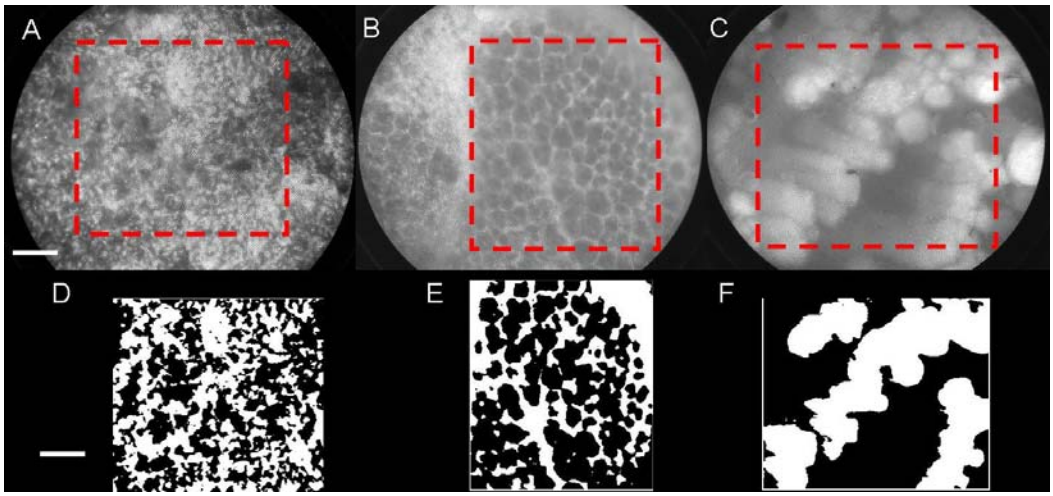

Figure 4. Homogeneous regions of interest, outlined in red, were selected within representative images of A) tumor, B) adipose, and C) muscle. D-F) Binary masks were applied to the regions within each image, from which parameters that capture morphological characteristics of tissue types can be calculated. Scale bar 100 µm.

An additional area in the quantitative image analysis approach we are exploring is characterizing the frequency content of homogeneous images in order to understand which frequency components are associated with muscle, tumor, and adipose. With this knowledge we hope to build a model that can diagnose a particular image as a specific tissue type or a combination of tissue types (i.e. 25% tumor, 75% muscle, and 0% adipose). An example case of using frequency and spatial information to separate tumor from muscle (and ultimately to detect residual disease) is shown in figure 2. A high pass filter is applied to the original image to remove the low frequency content of the muscle. Once the muscle is mostly removed, the image is converted to a binary image, which through the application of thresholding techniques, allows for isolation of the residual tumor nuclei from the underlying muscle. With the 55 images captured in this ex vivo study, we plan to train a diagnostic model based on automated feature extraction algorithms and apply this approach and methodology to images capture from clinical lumpectomy specimens.

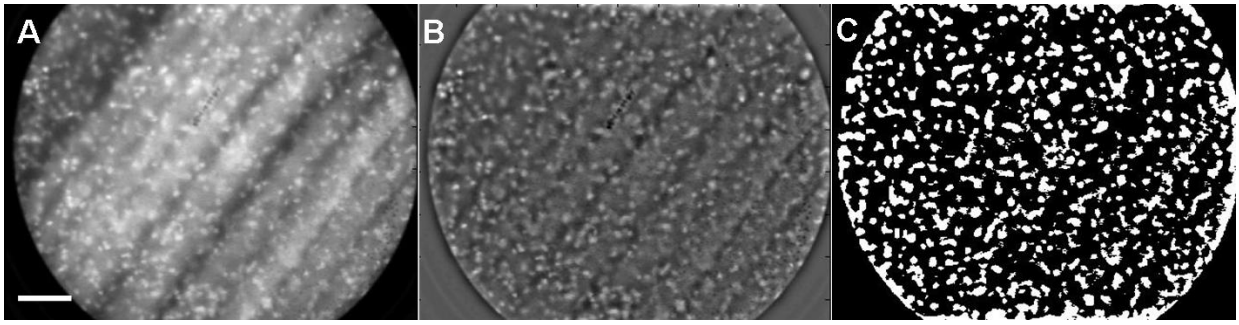

Figure 5. A) An image of tumor cells on top of longitudinal muscle fibers. B) The high pass filter applied to A) enables the isolation of the tumor nuclei, which once converted to C) binary form are readily apparent. Scale bar 100 µm.

2) *Ex vivo* clinical mastectomy study

As mentioned previously, we are pleased to report that we also conducted a small pilot study on mastectomy specimens, which enables us to more quickly assemble a “library” of representative high resolution fluorescence images (including invasive and *in situ* cancers). Having this library will inform how we apply the image analysis methodology discussed above to clinical breast margins, which will ultimately enable the automated detection of residual disease present on lumpectomy margins.

Methods:

Imaging protocol: For this pilot study, we consented patients undergoing a mastectomy. Immediately after the breast was removed from the patient, the collaborating pathologist inked the deep margin of the breast, and then bisected the tissue with a knife to expose the tumor

inside the breast. To be clear, no ink was present on the tumor or normal tissue on the inner surface of the cut tissue. Once the tumor was bisected, 0.01% (w/v) acriflavine (Sigma-Aldrich) dissolved in phosphate buffered saline (PBS) was applied topically to regions within the bisection (tumor) and to fatty regions surrounding the bisection (normal tissue). The distal end of the HRME fiber bundle was placed in contact with the tissue and images were acquired. Between each probe placement the distal end of the probe was cleaned with 55% ethanol.

Pathologic coregistration: During the imaging session specific sites of interest were inked with 1 mm dots for pathologic coregistration. After imaging and inking was complete, the tissue was returned for standard pathologic processing, and the resulting hematoxylin and eosin (H&E) stained slides were reviewed by an expert oncology pathologist who was blinded to the results of HRME imaging. For each inked area a diagnosis was given, which included invasive ductal carcinoma (IDC), ductal carcinoma in situ (DCIS), adipose, fibroadipose, fibroglandular, or any combination thereof.

Results:

Representative images: Four patients were consented in this study. Multiple images were taken from each site of interest yielding a total of 28 images from 3 fibroglandular, 2 fibroadipose, 1 adipose, 2 IDC, and 1 IDC/DCIS pathology confirmed areas or sites. Figure 6 shows representative images of all the tissue types mentioned. Large round adipocytes with nuclei pushed to the periphery of the cell, which is characteristic of adipose tissue, can be seen in Fig. 6A. Contrastingly in Fig. 6B string-like, densely packed collagenous structures with few nuclei can be readily seen. Fig. 6C shows a combination of round adipocytes and string-like collagenous structures indicating fibroadipose tissue. Both Fig. 6D and 6E show densely packed, disorganized nuclei, typical of IDC and DCIS.

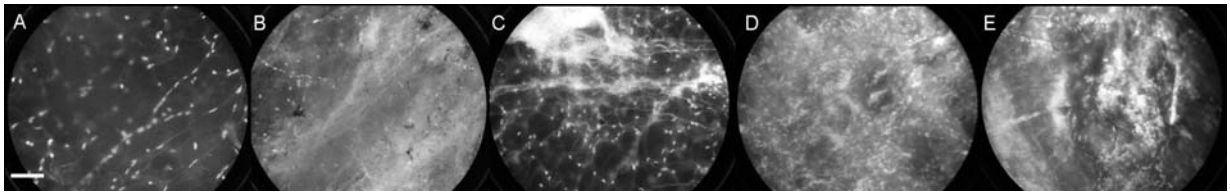

Figure 6. Representative images of A) adipose, B) fibroglandular, C) fibroadipose, D) IDC, and E) IDC/DCIS taken from ex vivo mastectomy specimens. Scale bar 100 μm.

It is also important to note that while there are differences between the murine sarcomas and clinical breast specimens, both margins are characterized by residual tumor cells surrounded by a normal milieu which include structural fibers and adipose tissue; the similarity between the human tissues and the pre-clinical model are shown in Fig. 7. Human mastectomy examples of A) tumor, B) adipose and C) fibrous tissue (specifically fibroglandular tissue) can be seen in the top row. Murine examples of D) tumor, E) adipose, and F) muscle fibers in a longitudinal section can be seen on the bottom row. As shown, both A) and D) have densely packed disorganized nuclei. Similarly B) and E) both are characterized by large round adipocytes; however, the human adipocytes are much larger than the murine adipocytes, as expected. This will make it even easier to distinguish tumor from adipose in clinical samples since the frequency content and structure of the adipose is more dissimilar from tumor in clinical sample than it is in murine samples. Finally, fibrous structures can be seen in C) human fibroglandular tissue and in E) murine muscle fibers in longitudinal section. While

we note there are some differences here, we believe that both C) and E) can be characterized by their low frequency content and therefore isolated or characterized in similar ways. These similarities between clinical and murine specimens support our approach to develop an image analysis methodology on murine sarcoma images, from which we can obtain a large sample of images rather quickly, and then to apply this same methodology of isolating tissue components via their frequency or textural content in clinical lumpectomy specimens.

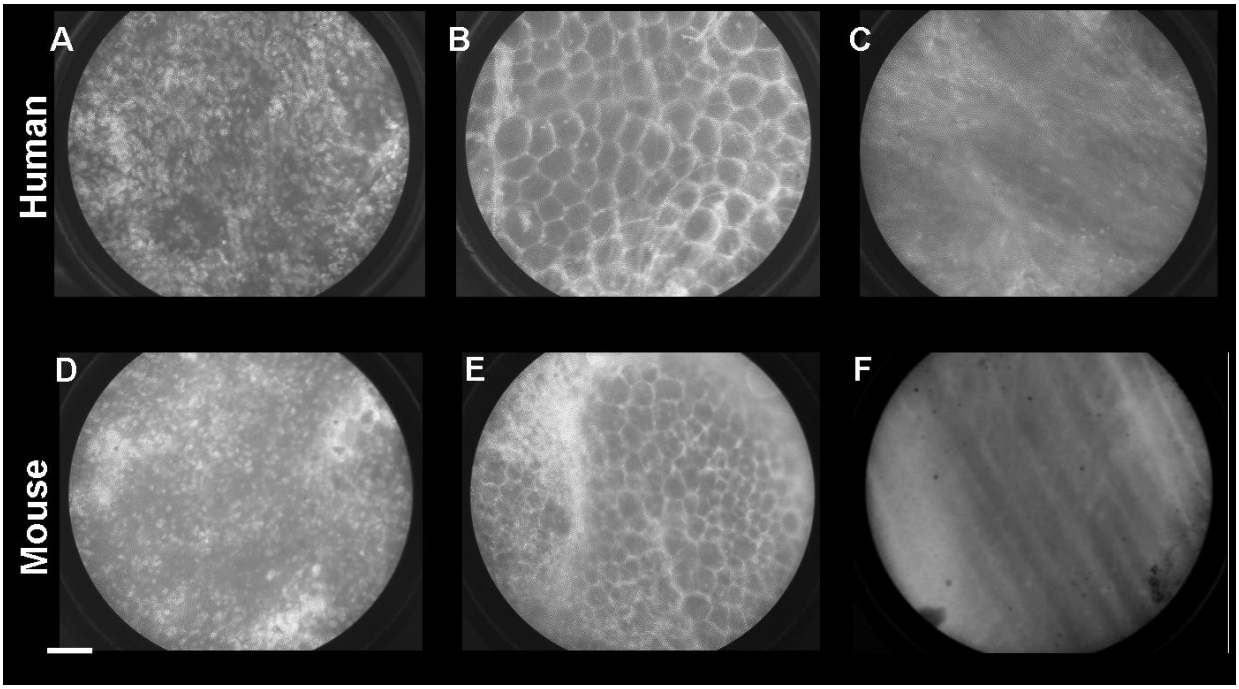

Figure 7. (A-C) HRME representative images, human breast, representing A) tumor, B) adipose, C) fibrous tissue. (D-F) HRME representative images, murine sarcoma, representing D) tumor, E) adipose, F) muscle tissue (longitudinal section). Scale bar 100 μm.

Through validating the image acquisition and analysis on murine sarcoma specimens and through completing a small pilot study on mastectomy samples, we feel confident in moving forward to start the 200 patient lumpectomy study. As discussed in the original document (and above), we plan to acquire data with both the spectral imaging platform and the HRME on the same clinical lumpectomy specimen to determine if we can improve our detection accuracy through harnessing the advantages of each approach.

B. Spectral imaging component: Wide-field Quantitative Diffuse Reflectance Imaging of breast tumor margins

Introduction: The second aspect of our proposed work in Aim 1 is to conduct a prospective validation study of our previously developed wide-field, quantitative diffuse reflectance imaging device, for detecting residual carcinoma at the margins of resected partial mastectomy

specimens. This clinical study on 200 patients is scheduled to commence in year 2 of the project. In Year 1, we have been preparing for this study in 2 primary areas: 1) technology refinement, and 2) algorithm development. Each area is described in more detail subsequently.

1) Technology Refinement Progress:

Previously, we conducted a study of our 8-channel quantitative diffuse reflectance imaging platform on over 100 patients at Duke University Medical Center. Preliminary results from the first 48 patients enrolled in this study were provided as preliminary results in the DOD Era of Hope application. This version of the device consisted of an 8-channel imaging probe array, which provided a coverage of 2 X 4 cm (approximately 8 cm^2), with 5 mm resolution. However, because most single breast margins routinely meet or exceed 20 cm^2 (or upwards of 100 cm^2 for the entire specimen), full coverage of the margins in this study required that the imaging probe be manually translated over the tissue surface, so that optical parameter maps of the tissue surfaces could be reconstructed. This process typically took as long as 20-40 minutes to image 1 or 2 surfaces of the specimen, which means that it was not generally possible to image the entire specimen surface.

To avoid this limitation for the prospective clinical study proposed in the DOD Era of Hope project in Aim 1b, we are developing a 49-channel version of the device concurrent to the DOD project. This second-generation device will allow full coverage of the specimen in 15 minutes allotted for intraoperative imaging. A schematic of the device is shown in Figure 8.

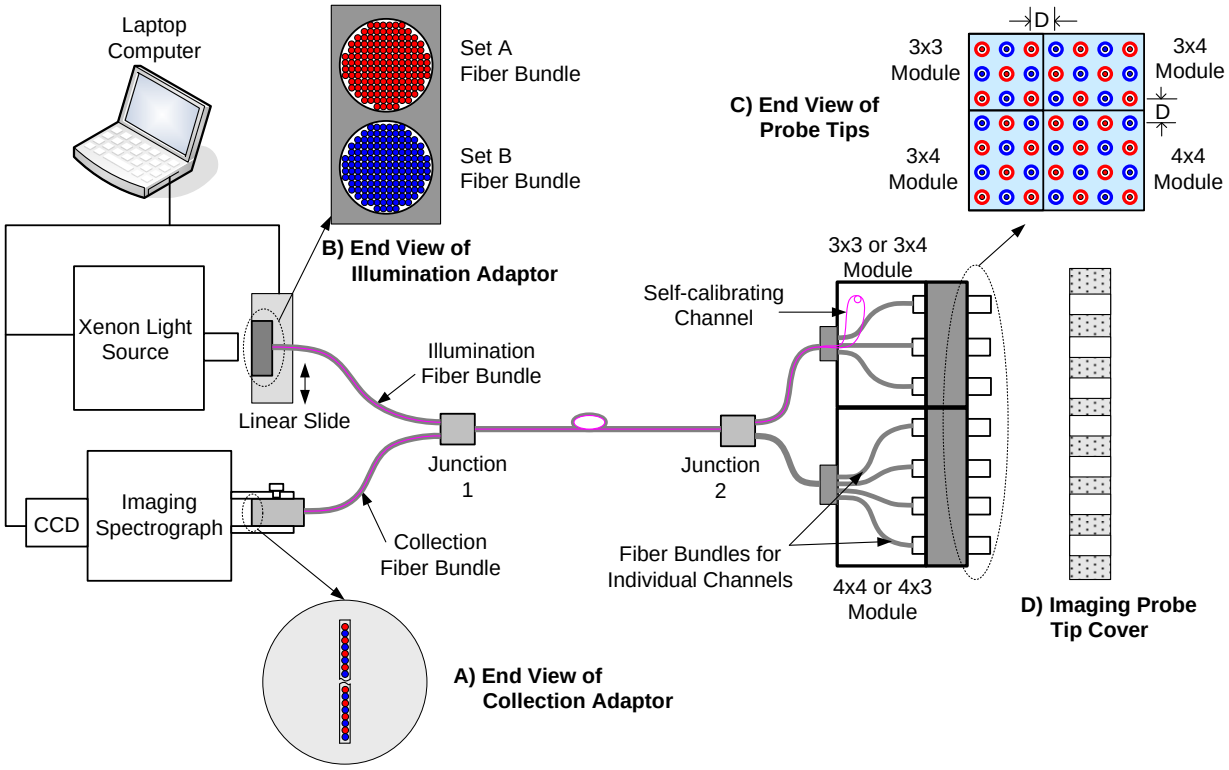

Figure 8. A 49-channel optical spectral imaging system: (A) arrangement of collection fibers to be imaged onto the CCD, (B) arrangement of illumination fibers in the illumination adaptor, (C) layout

of the common end, and (D) imaging probe tip cover made up of a plexi glass plate with a thin film layer to create a barrier with the imaging probe tip and the specimen.

The hardware for the 49-channel system has been assembled and tested, and we are currently awaiting fabrication of the custom 49-channel fiber optic imaging array. We anticipate that this will be completed by December 2010. A custom software package, which will provide real-time feedback (conversion of optical spectra to quantitative optical parameters), is being modified to incorporate the additional data channels, and should be completed by January 2010. With an additional month planned for probe testing and characterization, we anticipate that we will be able to begin recruiting patients for Aim 1b in February 2011. As described in the grant proposal, we will use real-time feedback from the imaging system to identify suspicious areas, which will be more closely investigated with the high resolution fluorescence imaging probe.

2) Algorithm development progress

Introduction: Since submission of the DOD Era of Hope proposal, we completed data collection from over 100 patients with the 8-channel margin imaging system. Since that time, we have been mining these valuable data to develop predictive algorithms which will be validated in the prospective clinical study under DOD funding.

As an initial step, we have decided to focus only on data from those patients who did not receive prior chemotherapy before their breast conserving surgery procedure (referred to as "chemo-naïve" patients). This is because it is known that chemotherapy can alter tissue composition in both normal and cancerous tissues, and we wanted to remove this as a source of variability. After excluding those patients, this resulted in margin images from 92 margins (46 negative margins and 46 positive margins) being retained for final data analysis. There are a number of ways in which these data could be exploited to develop a predictive model for margin status. One way is a **site-level analysis**, in which data from each pixel on the margin are considered separately in a predictive model, which is trained on data from pixels with a pathology-confirmed diagnosis. This requires data from an equal (or comparable) number of spectra from normal tissue as well as positive sites (containing residual cancer), in order for a robust predictive model to be developed. However, due to the focal nature of residual cancer at lumpectomy margins, most of the path-confirmed pixels in our study were from negative sites (which did not contain cancer). While these data are useful in what they can tell us about the sources of contrast in the normal breast, they are not that useful in developing site-level prediction algorithms that that provide the probability that a given pixel on a margin actually contains cancer. Thus, a second approach, is to consider a **margin-level analysis**, in which the entire margin map (i.e., all pixels measured on a margin) are compared to the pathologic margin status; that is, whether the margin was positive or negative for residual cancer within 2mm of the tissue surface. Because we have an equal number of negative and positive margins in this case, prediction algorithms trained on these data are expected to be more robust and valid. However, this poses a new challenge; namely, how does one best exploit the information content present in a given image, when little is known about the location or extent of residual disease on that margin? To this end, we have developed a systematic procedure for reducing the information in the image to scalar values which are easily incorporated into various

multivariate prediction algorithms. The following sections describe the methodology and results from this margin level analysis.

Methods: The margin imaging protocol and details on the spectral analysis routines can be found in described in detail in our published manuscripts REF. Briefly, the imaging probe was interfaced to the lumpectomy specimen through an acrylic container, with holes drilled for insertion of each channel of the probe, allowing the probe tips to just come in contact with the tissue. Figure 9 contains a photograph of the imaging probe interfaced with the specimen container during imaging of a mock lumpectomy specimen. The probe tips are designed such that they extend about 1mm past the inner surface of the container, providing a reproducible probe-tissue contact. A single placement of the probe array collects data from 8 container holes (or pixels). The entire margin surface was imaged by manually translating the position of the imaging probe horizontally and vertically until data from all of the holes were obtained.

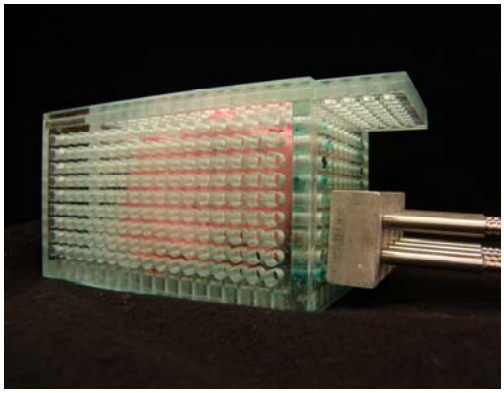

Figure 9. Photograph of the 8-channel imaging probe interfaced with the adjustable specimen container.

For a small margin, approximately 4 placements of the probe were required to image the entire margin (requiring up to 100s total acquisition and processing time), and for a large margin up to 16 placements were required (requiring up to 400s total acquisition and processing time). Images of the margins were reconstructed with the extracted absorber concentrations and scattering parameters. In addition to maps of the concentrations of oxy- and deoxy-hemoglobin and β-carotene, and the wavelength-averaged reduced scattering coefficient, $<\mu_s'>$, maps of the wavelength-averaged reduced albedo (wavelength average of the quantity $\mu_s' / (\mu_s' + \mu_a)$), and ratios of absorber concentrations and $<\mu_s'>$, were also computed.

Results and Discussion: In order to develop an algorithm for margin classification, margin parameter images were reduced to scalar image descriptive variables amenable to predictive model construction. This consisted of taking an image of the margin representing a particular optical parameter (selected from wavelength-averaged $<\mu_s'>$, $<\mu_a>$, and <reduced albedo>; total hemoglobin concentration, β-carotene concentration, and ratios of total hemoglobin and β-carotene concentration to $<\mu_s'>$), and computing a summary statistic which reduced the image to a single value. A number of statistical summary variables, such as the mean, variance,

covariance, minimum, maximum, and range of the image, were considered. Ultimately, two statistical summary variables were considered for further analysis. One was the median value of each optical parameter over the entire image. The second is related to the distribution of values in the image, and is given by computing the percentage of image pixels which lie below a pre-defined threshold. For each optical parameter, 20 thresholds were chosen, such that for each margin, there were 7 optical variables X 21 statistical measures = 147 total variables. The selection of thresholds was determined empirically for each optical variable, and was based on the concept of data quantiles. For each optical variable, all pixels from all margins (4953 pixels) were used to compute 20 quantiles on the data distribution, from 0.05 to 0.95 in 0.05 increments. In other words, the optical parameter values corresponding to the 5th through to the 95th percentile, in 5 percentile increments, were computed. These data quantiles were then selected as the threshold values for that particular optical variable, which were then used in computing the percent-pixel quantities for each individual margin image. That is, for each margin image and optical parameter, the percentage of image pixels that lies below each of the 20 thresholds was computed for that margin, resulting in 20 “percent-pixel” variables for that particular margin image.

In this approach, the thresholds chosen were selected to be evenly spaced over the distribution of values for all pixels from all margins combined. This approach was chosen rather than choosing thresholds evenly spaced over the data range, because the distributions of values for each optical parameter were generally non-Gaussian. This is demonstrated schematically in Figure 10. As seen in the figure, choosing thresholds based on the data quantiles results in a more efficient division of the data, than if the thresholds were chosen based on the data range. In effect, this thresholding technique is an efficient means to compare the data distributions of the margin images, and is based on the observation that the empirical cumulative distribution functions (CDF) for all pixels from negative margins is different from the empirical CDF for all pixels from positive margins, for many of the optical variables under consideration (see Figure10 for one example).

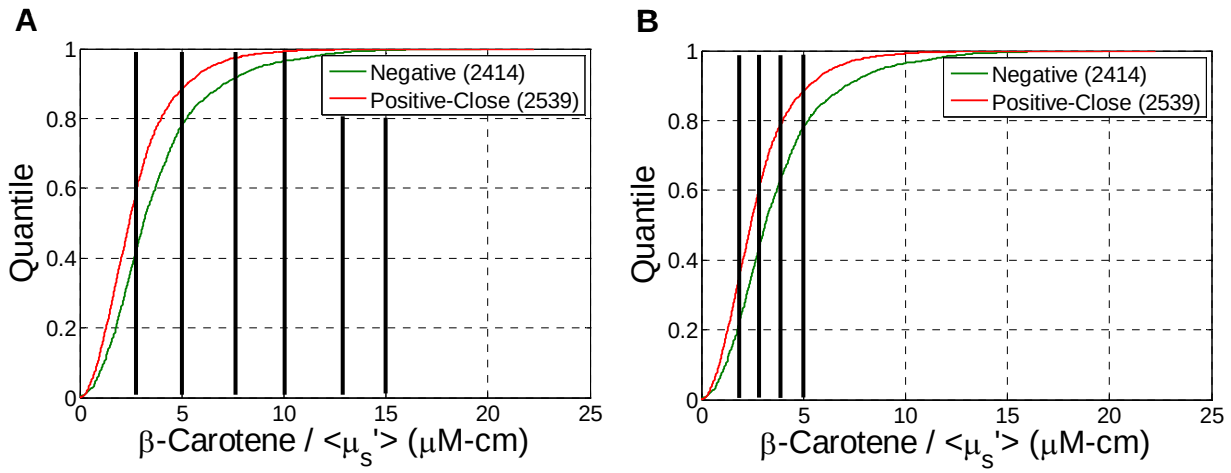

Figure 10. Empirical cumulative distribution function of the ratio of β-carotene to the wavelength-averaged scattering coefficient, $<\mu_s'>$, for all pixels from all negative margins and all pixels from

positive/close margins. A) The first item of note is that the distributions are different, which is the basis for the thresholding approach used in the image reduction scheme. Note that if the thresholds (indicated by vertical lines) were chosen evenly over the x-axis (the data range), that thresholds above 10 would only be relevant to less than 2% of the samples. B) However, choosing the thresholds evenly over the y-axis (the data quantiles), ensures that the thresholds evenly sample the data distribution, even though most of the threshold values are centered in the lower values of the data range.

To summarize, the resulting dataset is comprised of the median image value for each optical parameter, for each margin image. In addition, for each optical parameter image there are 20 variables, corresponding to the percentage of image pixels below each of the 20 thresholds. However, for each optical variable, we want to retain only one of these pixel percentage variables for use in a predictive model. To select the best percent-pixel variable, which reflects the threshold which best separates the positive and negative margin distributions, we calculate the Wilcoxon rank-sum test between positive and negative margin images, for each percent-pixel variable. The percent-pixel variable with the lowest *p*-value was then retained, such that the final dataset comprised 1) the median image value for each margin image, and 2) the best percent-pixel variable for each margin image. This resulted in 7 optical parameters X 2 statistical variables = 14 total variables retained for construction of a predictive model.

We chose to use conditional inference trees for construction of a predictive model for margin status based on these data. Conditional inference trees are a decision-tree based approach which relies on recursive partitioning of samples in a conditional inference framework. This allows for automated selection of candidate predictor variables in an unbiased manner. Because a Wilcoxon rank-sum test is used at each node in the decision tree, conditional inference trees are robust to overfitting and do not require pruning or cross-validation, unlike other decision-tree models. Another advantage of conditional inference trees is that they allow for inclusion of clinical or demographic parameters into the conditional inference framework, such as breast density or menopausal status.

Figure 11 contains the resultant conditional inference tree from the dataset previously described. The first node of the tree is the percentage of β-carotene/$<\mu_s'>$ margin image pixels below 1.71. As shown in the right branch of node 1, if more than 22.6% of the margin image pixels are below 1.71, then the samples were placed in terminal node 7. Terminal node 7 is comprised of 40 samples overall, with 29 positive margins and 11 negative margins (as indicated by the bar chart which shows the diagnostic breakdown of samples in that node). This indicates that node 7 represents a positive conditional class probability (CCP) of 73%, and that any future sample placed in this node would be classified as "positive," with a 73% probability of being a true positive. The same process can be used to trace the decisions on the left branch of node 1. As seen in the tree, all of the samples can be efficiently classified using only 2 additional variables: the median $<\mu_s'>$ (scattering) value in the image, and the median THb (total hemoglobin) value in the image. Terminal nodes 4 and 5 represent samples that are predominantly negative and new samples placed in those nodes will be classified as such, whereas terminal nodes 6 and 7 represent samples that are predominantly positive. The confidence that a future sample will be classified correctly can be estimated by observing the conditional class probabilities for each terminal node. For example, new samples placed in

terminal node 5 are very likely to result in a true negative, since the negative CCP = 100%. However, samples placed in terminal node 4 could result in a false negative, since the negative CCP = 56%. The effect of this on the overall classification accuracy is also a function of how many samples are classified in a particular node. For example, although samples classified in terminal node 4 have a 44% probability of being misclassified, the fraction of samples classified in that node is only 16/92 or 17%. On the other hand, the terminal node which represents the greatest number of samples at 40/92 or 43%, terminal node 7, gives a 73% probability of a correct true positive classification.

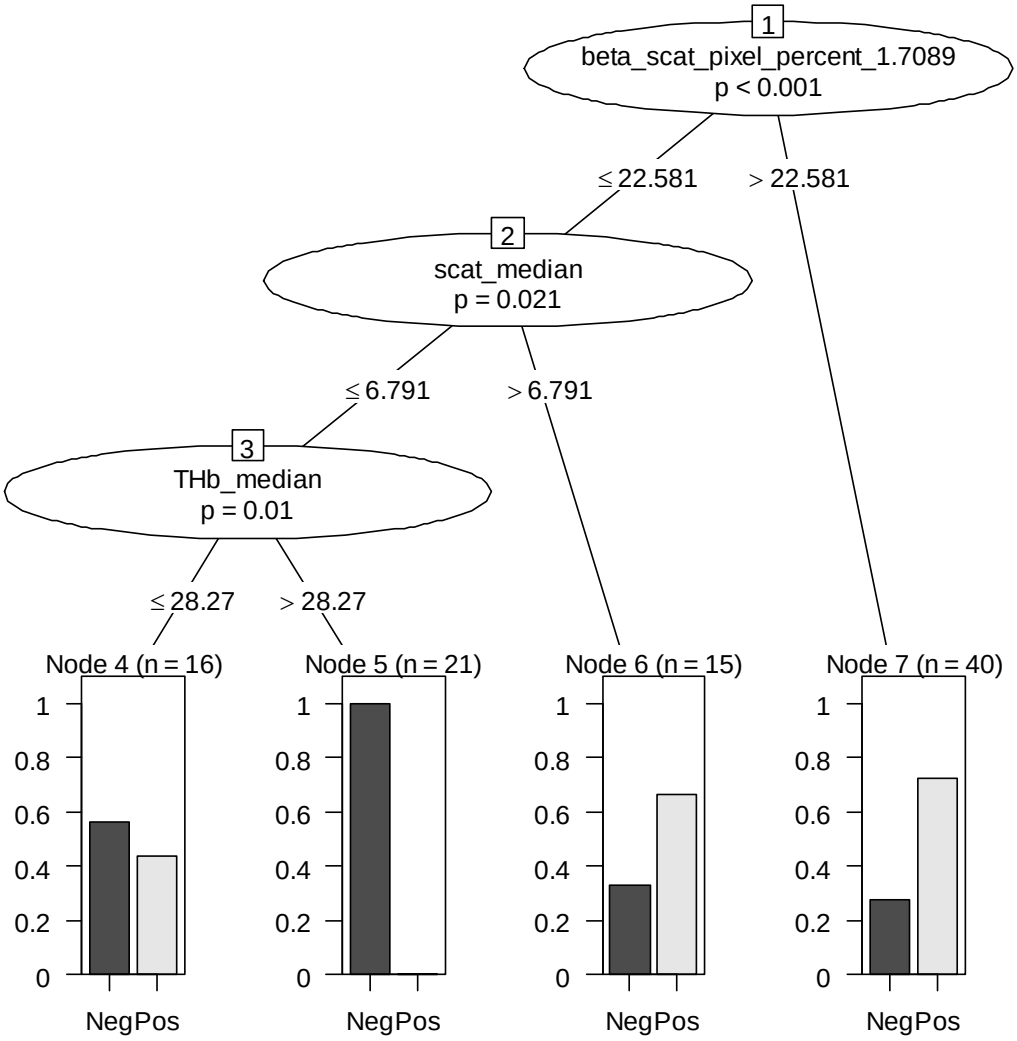

Figure 11. Conditional inference tree model for prediction of margin status.

Table 4 contains estimates of the prediction accuracy for margin status using the conditional inference tree model. This predictive algorithm results in an overall classification accuracy of 75%, with a sensitivity of 85% and a specificity of 65%. For the purposes of breast conserving surgery, the objective of any intraoperative margin surveillance tool is to catch all positive margins (thereby eliminating the need for a re-operation), while not causing unnecessary

removal of tissue (since the goal of BCS over mastectomy is to conserve breast cosmesis). The balance between false negatives and false positives, and which are preferable is a debatable one. On the one hand, the risk of a false negative is to leave cancer in a patient that will cause another operation, or even worse, a recurrence of the tumor. Conversely, the risk of a false positive is that additional tissue may be taken that could be associated with poor breast cosmesis or other associated co-morbidities. In our particular case, use of the device could result in a greatly reduced re-operation or recurrence rate, at the potential risk of removing tissue unnecessarily.

Table 4. Prediction accuracy for the conditional inference tree model.

Sensitivity	Specificity	PPV	NPV	Accuracy
85	65	71	81	75

We have also been investigating the natural variability in optical sources of contrast in normal breast tissue. It is important to understand how patient-to-patient variability affects the contrast between normal and cancerous tissue for each optical parameter measured by our imaging modality. We have uncovered a number of relationships between patient demographic or clinical factors with optical parameters. For instance, we found that the mean $<\mu_s'>$ of a margin image is correlated with the mammographic breast density of the breast from which it came; specifically, more dense breasts were associated with higher optical scattering (Figure 12). This is likely due to the increased collagen content in denser breasts, which is expected to contribute to higher optical scattering coefficients. Therefore, we are investigating the inclusion of demographic or clinical patient factors into the conditional inference tree framework. For instance, if breast density is able to separate groups of patients on the basis of which optical variables demonstrate highest tumor to normal contrast in that subgroup of patients, then the conditional inference tree modeling approach will aid us in that determination. This work is in progress.

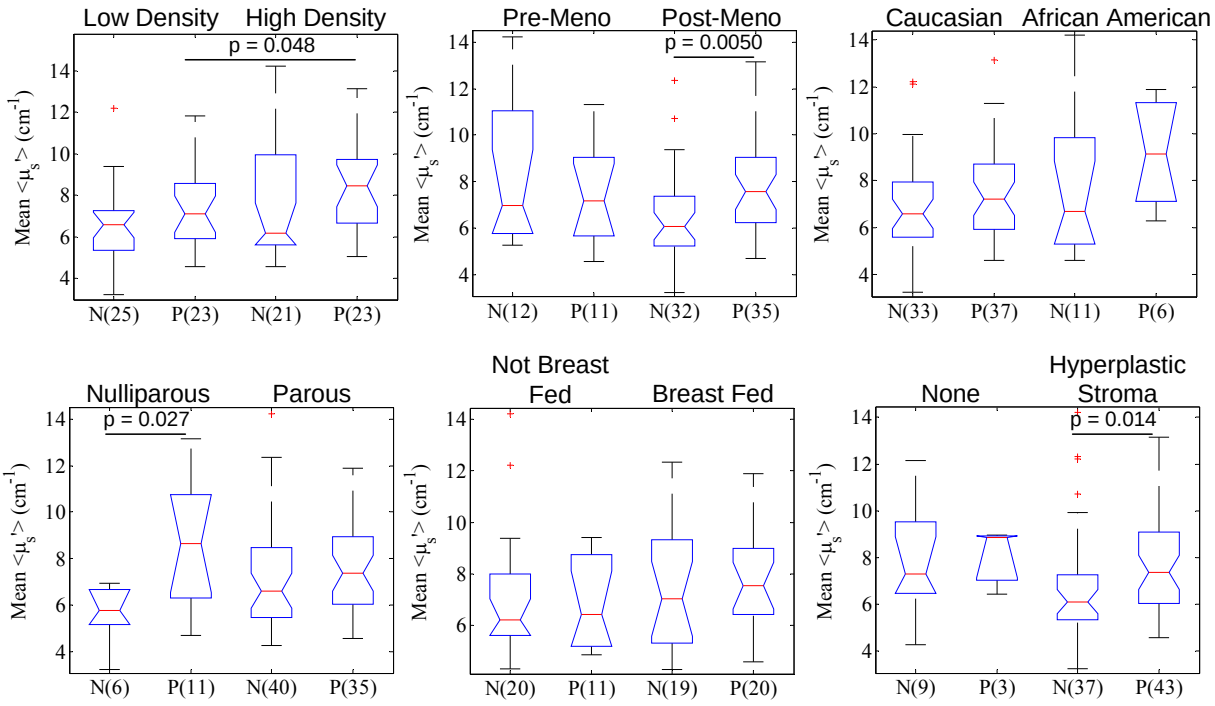

Figure 12. Boxplots of the mean scattering (<μ_s'>) of negative (N) and close/positive (P) margins for radiographic breast density, menopausal status, race, parity, breast feeding, and changes in the benign stroma. The breast feeding data is only taken from parous women.

Plans for Year 2: In year 2 of the project, we will complete the development of the 49-channel imaging device, and begin recruiting patients into the margin imaging protocol. Patients undergoing an initial partial mastectomy procedure will be recruited into the study.

Aim 2: Optical quantitative biology of different breast cancer subtypes.

Introduction: The objective of the work in Aim 2 is to use optical spectroscopy to measure optical markers of tumor microenvironment in women with cancers representing a wide variety of molecular subtypes, and to determine whether these optical measures can be predictive of eventual chemotherapy response in a subset of the patients who are measured prior to commencement of chemotherapy. The 150-patient clinical study proposed in Aim 2 is not scheduled to begin until Aim 2 of the project. In Year 1, we have been preparing for this clinical study by 1) designing and acquiring a custom needle-compatible optical probe, 2) identifying critical workflow junctions in the breast cancer care system at Duke University so that we can most efficiently target the highest number of eligible patients possible for recruitment, and 3) completing necessary IRB approvals.

Methods: Based on our prior experience and discussions with our collaborators, we decided to develop a forward-firing optical probe (rather than the side-firing probe mentioned in the proposal), based on the desire to recruit patients undergoing an ultrasound-guided biopsy. Ultrasound guidance is used for patients who are undergoing a pre-therapy biopsy of a diagnosed cancer at Duke, and is also used in any biopsy procedure that is performed in the operating room. Since the biopsy devices that are commonly used with ultrasound guidance

employ forward-facing apertures (as opposed to those needles designed for X-ray guided stereotactic biopsy, which have side-firing apertures), we decided to go with a forward-firing probe to ensure compatibility with the procedures under which we can enroll the most patients.

Results: We have developed a 14-gauge biopsy-needle-compatible optical spectroscopy probe that when inserted into a lesion under image guidance can non-destructively and within seconds assess the tumor micro-environment to a depth of several millimeters from the tip of the probe (Figure 13). We specifically designed the optical probe to be compatible with the Bard Vacora handheld, vacuum-assisted biopsy system, which is used by the Duke Radiology Breast Imaging Center for ultrasound guided biopsies, and can also be transported to the operating room since it is a handheld portable device.

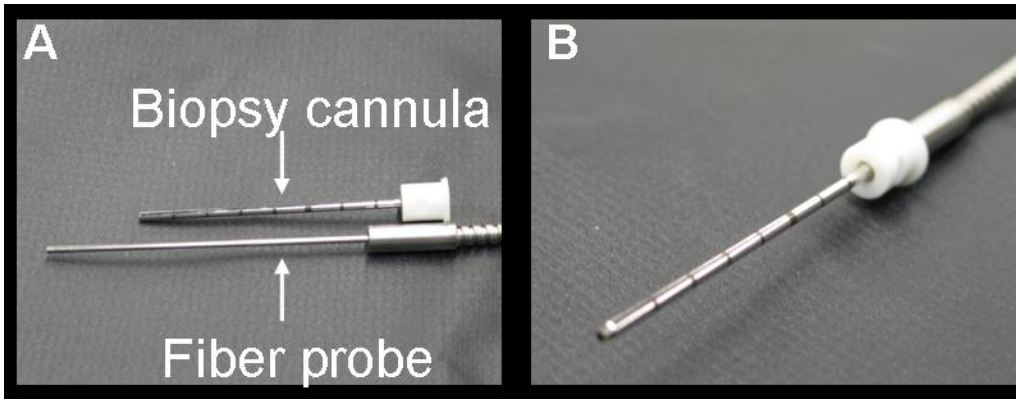

Figure 13. Photographs of A) the custom 14G optical spectroscopy probe and a Bard Vacora biopsy cannula, and B) the probe inserted into the cannula. In our protocol, the cannula will be placed into the tumor under ultrasound guidance, which will provide a means to interface the spectroscopy probe with the tumor in vivo.

We are also pleased to report progress towards the clinical goals of Aim 2. It is important to note the clinical studies proposed in Aim 2 are not scheduled to begin until year two. During year one, we have succeeded in moving this aim forward though we have faced several challenges in the process. The first challenge we face is the time required to write, submit, and receive approval for the human subjects protocol and informed consent form. In July of 2009, we began the IRB approval process with the Department of Defense, Duke University and the subcontracting institution, Rice University. For the next seven months we iterated on the protocol with the DoD and Rice University. Near the end of February, 2010 the three organizations agreed on content of the protocol and the final protocol was submitted to Duke University Health Systems (DUHS) for IRB approval. DUHS IRB approved the protocol on March 30th, 2010. We have been able to enroll patients since the DoD granted their final approval for the study on April 1st, 2010.

The second challenge we face is working with multiple institutions for IRB approval. During the review of the protocol, the Rice IRB deemed their institution engaged in human subject research. This came as a surprise to the study team since Rice University is not a patient enrolling site. As a result, the protocol required approval by the Rice IRB in addition to DUHS IRB approval. Rice University approved the protocol on April 21st, 2010.

The third challenge we face is the cost of conducting research with the Pathology Department at Duke University. This proposal was routed through the University and submitted to the DoD on January 21st, 2009. At that time the Pathology Department was not charging a fee for processing research specimens. Presently, the Pathology Department is requesting a fee for each research specimen they process. We are currently negotiating these terms and hope to reach an agreement in the near future. As a result, a rebudget will be required for years 2-5 to account for the specimen processing fee the study will incur.

Plans for Year 2: In year 2 of the project, we will commence the recruitment of subjects into the clinical studies. Patients who are undergoing either a simple or partial mastectomy for a chemo-naïve tumor will be recruitied. In addition, patients undergoing a pre-therapy biopsy for selection of chemotherapy regimen will also be recruited.

Aim 3: *Optical quantitative biology to assess therapy response in different sub-types of breast cancer:*

The research goals for aim 3a have altered slightly from the original statement of work. As proposed, murine window chambers have been implemented for the intra-vital monitoring of hemoglobin saturation and fluorescence. However, the mouse model has been changed to a murine mammary carcinoma that is constitutively labeled with red fluorescence protein, 4T1-RFP. This model allows for co-registration of the tumor area and fluorescence. Also, in our previous studies, our group has demonstrated that the metabolic fluorescent contrast agent 2-[*N*-(7-nitrobenz-2-oxa-1,3-diazol-4-yl)amino]-2-deoxy-D-glucose (2-NBDG) can be used to delineate therapeutic responders from non-responders by measuring changes in glucose use (Millon et al.). Therefore, for the early studies, we are utilizing 2-NBDG to monitor changes in glycolysis and oxygenation caused by hypoxia.

Introduction: Glycolysis is the first step in energy creation during metabolism for all living things and the glycolytic products are used for oxidative phosphorylation if oxygen is present. If oxygen is low or not present it is referred to as hypoxia and increased glycolysis is necessary. Hypoxia has long been associated with cancer and prolonged hypoxia has been associated with further cellular disregulation. Hypoxia has been suggested as one potential cause of the Warburg effect. The Warburg effect is increased glycolysis in the presence of oxygen and is associated with increased radio and chemoresistance. To determine whether metabolism is dominated by the Warburg effect or Pasteur, glycolysis and oxygenation must be known. The ability to non-invasively detect tissue that has increased glycolysis even in the presence of oxygen could help with cancer prognosis and treatment planning. Therefore we first tested the effect of hypoxia on 2-NBDG in vitro with chemically simulated hypoxia, chronic hypoxia and cycling hypoxia. Cycling hypoxia has been previously shown to have a greater impact on tumor environment and was implemented in an in vivo murine dorsal window chamber mammary carcinoma model. Oxygenation and glycolysis were both quantified to determine if differences exist.

Methods: 4T1-RFP cells were treated with chemically simulated hypoxia, chronic hypoxia (0.5% oxygen for 24 hours) or cycling hypoxia (3 cycles of 1 hour of 0.5% oxygen and 1 hour in

normoxia at 21%). Normoxic controls (21% oxygen) for all 3 groups were tested simultaneously. After treatment or controls the cellular uptake of 200 μM 2-NBDG was measured via confocal microscopy. The cells were labeled with 2-NBDG for 20 minutes prior to washing and then imaged. Fluorescence intensity was quantified and compared between treated and normoxic controls.

4T1-RFP cells were then implanted in murine window chambers and allowed to grow for 6 days. Normal mice (no cells implanted) were used as controls. Both groups of mice were then subjected to 3 cycles of 1 hour in 10% oxygen and 1 hour 21% oxygen (6 hours total) or allowed to remain in 21% oxygen for the 6 hours prior to imaging as normoxic or cycling hypoxic. N=12 mice with 3 mice per group (normoxic normal, normoxic tumor, cycling hypoxic normal, cycling hypoxic tumor). Cycling hypoxia should cause an increase in glycolysis in normal and tumor since the Pasteur effect will be forced, and cycling hypoxia in normal will allow for exclusion of tumor perfusion effects as the cause of 2-NBDG uptake. Absorption images to determine tumor oxygenation, baseline green fluorescence and red fluorescence were obtained with an intra-vital microscope. 2-NBDG was then injected via tail-vein at a concentration of 200 μg/mL and images of the change in green fluorescence were obtained every 5 minutes for 60 minutes. The uptake of 2-NBDG was quantified and correlated with the hemoglobin saturation values found at baseline to determine the main metabolic process.

Results: Simulated, chronic, and cycling hypoxia all showed a significant increase in 2-NBDG uptake in vitro as compared to the normoxic cells. The uptake of 2-NBDG in vivo was then tested. Fluorescence intensity changes over 60 minutes showed 2-NBDG uptake was significantly greater in normoxic tumor tissue than normoxic normal tissue. Cycling hypoxic tumor and normal 2-NBDG uptake was not significantly different from one another, but both had significantly greater uptake than the normoxic counterparts. The uptake of 2-NBDG at t=20 minutes was then further examined in the 4 groups to determine if the addition of glycolysis to baseline oxygenation measurements could help determine metabolic processes. Figure 14 shows the measurements alone and how the inclusion of glycolysis and oxygenation provides the clinician with more pertinent information.

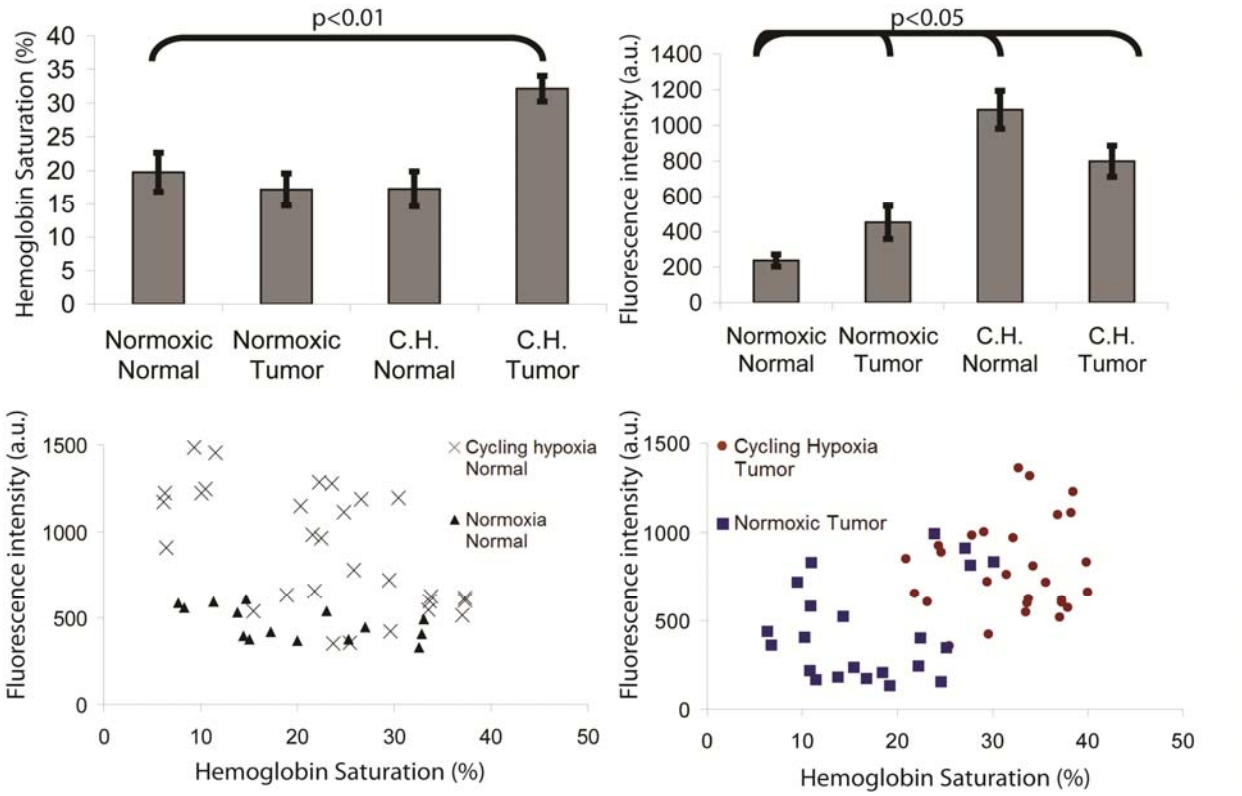

Figure 14. The mean and standard error of oxygenation alone, 2-NBDG fluorescence intensity and then scatterplots of the combined hemoglobin saturation versus fluorescence intensity for normal and tumor.

These tests demonstrate that 2-NBDG has potential to be exploited for discrimination of cancer and normal and furthermore have the ability to determine whether the tissue has low oxygenation and high glycolysis (Pasteur dominated) or high oxygenation and high glycolysis (Warburg dominated).

Plans for year 2: In Year 2, the window chamber models will be used to look at the immediate effects of radiation and chemotherapy treatments. To determine long term effects, we will also implant flank tumors into mice and determine if our previously established first that the fluorescence model accurately detects 2-NBDG. After, we will then implant and treat the flank tumors with radiation or chemotherapy to determine if 2-NBDG uptake is directly associated to long term tumor response and correlate it directly with hemoglobin saturation.

3. KEY RESEARCH ACCOMPLISHMENTS:

AIM 1

- Demonstrated high resolution microscopy (HRME) combined with proflavine can be used to qualitatively detect residual disease at surgical murine sarcoma margins.
- Demonstrated the potential of several approaches for quantitative analysis of HRME images including calculating raw parameters from gray-scale images (mean intensity, standard deviation, skewness), converting images to binary form and then calculating

parameters that reflect tissue morphology (feature size and density), and isolating tissue types through filtering in the frequency domain.
- Assembled a HRME image library of various tissue types found in the breast through completing an *ex vivo* pilot study on clinical mastectomy specimens. Imaged tissue types include adipose, fibroglandular, fibroadipose, IDC, and IDC/DCIS tissues.
- Development of 49-channel quantitative spectral imaging device for margin assessment
- Development of margin prediction algorithms to be tested in the 200-patient clinical study
- IRB-approved protocol to conduct clinical studies

AIM 2

- Development of specialized optical probe to be used through a forward-firing breast biopsy needle under ultrasound guidance
- Identification of key clinical procedures and clinicians at Duke which will aid in patient recruitment
- IRB-approved protocols to conduct clinical studies

AIM 3

- 2-NBDG uptake is significantly increased after simulated, chronic and cycling hypoxia in vitro.
- 2-NBDG uptake is significantly greater in normoxic tumors as compared to normoxic normals.
- Cycling hypoxia causes an increased uptake in 2-NBDG as compared to all normoxic tissue.
- The combination of glycolysis measurements and oxygenation data allows for determination of the dominant metabolic pathway.

4. REPORTABLE OUTCOMES:

AIM 1:

We plan to submit the article “High resolution microendoscope for surgical margin assessment demonstrated in a murine sarcoma model” to a scientific journal by December of this year. Much of the data for this article was discussed above; however, we are still exploring various pre-processing techniques in order to determine the best quantitative image analysis approach for the HRME data.

1. Mueller J, Mito J, Kim Y, Geradts J, Kirsch D, Ramanujam N, Brown JQ, “High resolution fluorescence imaging for tumor margin assessment demonstrated in a murine soft tissue sarcoma model,” in preparation.

In addition, we have applied for additional funding from the NIH to develop a high-throughput *in vivo* microscopy tool, which could potentially replace the HRME tool currently used in this work. An advantage of the HRME tool is its high resolution and quasi-optically sectioned image collection; however, its major disadvantage is its very small footprint, relative to the size of typical breast margins. We have proposed to develop a non-contact, large-field sectioning microscope, for high-throughput microscopic scanning of tumor beds *in vivo*. This device would

increase the effective single-shot field-of-view of the microscope by a factor of six, while removing the need to manually scan a probe over the tissue surface by allowing non-contact raster scanning of the tissue surface. This would allow the full surface of the margin to be examined microscopically in a clinically-relevant timeframe for intraoperative imaging. The data obtained with DOD funding (described above), was used as preliminary data in this R21 proposal. This NCI proposal was scored at the 6th percentile, with council review occurring in January 2011.

We also plan to submit 2 manuscripts by December of this year resulting from the analysis of the quantitative spectral imaging data previously collected. One manuscript will detail the development of margin prediction algorithms, and the other will detail the correlations between optically-measured biomarkers and variations in normal breast tissue type.

2. Brown JQ, Barry WT, Bydlon TM, Kennedy SA, Junker M, Gallagher J, Geradts J, Wilke LG, Ramanujam N, "Quantitative diffuse reflectance imaging of breast tumor margins: Comparison of margin status prediction algorithms," in preparation.
3. Bydlon TM, Kennedy SA, Brown JQ, Gallagher J, Junker MK, Barry WT, Geradts J, Ramanujam N, Wilke LG, "Effects of patient characteristics on the optical properties of neoadjuvant naïve breast tumor margins," in preparation.

AIM 2:

None

AIM 3:

1. Millon SR, Fontanella AF, Ostrander JH, Brown JQ, Dewhirst MW, Ramanujam N. "Potential use of 2-NBDG to identify hypoxic tumors." In preparation.

5. CONCLUSION:

Aim 1a, High resolution Imaging:

The *ex vivo* murine pilot feasibility study demonstrates that high resolution imaging of acriflavine stained tissue is a potential tool for rapid detection of margin positivity in an intra-operative setting with the goal of reducing re-excision rates and over-treatment. Furthermore, preliminary quantitative image analysis shows promise for isolating individual tissue types and ultimately could allow for the automated detection of residual disease of surgical margins. Based on our preliminary analyses, we believe that the image specifications of the HRME device (particularly regarding SNR and resolution) are appropriate for detection of residual carcinoma at the surgical margin.

Aim 1b, Wide-field quantitative spectral imaging:

An algorithm which predicts pathologic tumor margin status based on intraoperative quantitative diffuse reflectance imaging of the specimen has been developed on data collected in a prior study. This algorithm, based on a conditional inference tree technique, has an estimated accuracy of 85% sensitivity and 65% specificity, and will be validated in the prospective 200 patient clinical study proposed in Aim 1b of the DOD project. Concurrent to the DOD-funded work, a next-generation spectral imaging device is being developed which will greatly increase the speed of intraoperative imaging, and will facilitate the proposed 200 patient clinical study.

Aim 2

The objective of the work in Aim 2 is to use optical spectroscopy to measure optical markers of tumor microenvironment in women with cancers representing a wide variety of molecular subtypes, and to determine whether these optical measures can be predictive of eventual chemotherapy response in a subset of the patients who are measured prior to commencement of chemotherapy. The 150-patient clinical study proposed in Aim 2 is not scheduled to begin until Aim 2 of the project. In Year 1, we have been preparing for this clinical study by 1) designing and acquiring a custom needle-compatible optical probe, 2) identifying critical workflow junctions in the breast cancer care system at Duke University so that we can most efficiently target the highest number of eligible patients possible for recruitment, and 3) completing necessary IRB approvals.

Aim 3

Hypoxia is shown first in vitro to increase 2-NBDG uptake. Simulated, chronic and cycling hypoxia were completed in vitro with subsequent increases in 2-NBDG as well. The uptake of 2-NBDG in tumor and normal tumor-free tissue was tested and 2-NBDG discriminated normal from tumor in a normal oxygen environment. An increase in 2-NBDG was demonstrated after cycling hypoxia in tumor and normal tissue. However, by including hemoglobin saturation data, cycling hypoxic tumor tissue can be discriminated from cycling hypoxic normal tissue and normoxic tumor tissue. From these experiments, the applicability of 2-NBDG as a method to monitor changes in glycolysis and its increased potential by including hemoglobin

6. REFERENCES:

1. Kumar, V., A. Abbas, and N. Fausto, *Robbins and Cotran Pathologic Basis of Disease*. 7th ed. 2005, Philadelphia: Elsevier Saunders.

2. Muldoon, T.J., et al., *High-resolution imaging in Barrett's esophagus: a novel, low-cost endoscopic microscope.* Gastrointest Endosc, 2008. 68(4): p. 737-44.

3. Muldoon, T.J., et al., *Subcellular-resolution molecular imaging within living tissue by fiber microendoscopy.* Opt Express, 2007. 15(25): p. 16413-23.

4. Kirsch, D.G., et al., *A spatially and temporally restricted mouse model of soft tissue sarcoma.* Nat Med, 2007. 13(8): p. 992-7.

5. Ferguson, L.R. and W.A. Denny, *The genetic toxicology of acridines.* Mutat Res, 1991. 258(2): p. 123-60.